Ultracold quantum dynamics: spin-polarized K + K_2 collisions with three identical bosons or fermions

Goulven Quéméner, Pascal Honvault, Jean-Michel Launay,
UMR 6627 du CNRS, Laboratoire de Physique des Atomes, Lasers, Molécules et Surfaces, Université de Rennes, France

Pavel Soldán, Daniel E. Potter, and Jeremy M. Hutson
Department of Chemistry, University of Durham, South Road, Durham, DH1 3LE, England

(Dated: February 2, 2008)

We have developed a new potential energy surface for spin-polarized $K(^2S)$ + $K_2(^3\Sigma_u^+)$ collisions and carried out quantum dynamical calculations of vibrational quenching at low and ultralow collision energies for both bosons ^{39}K and ^{41}K and fermions ^{40}K. At collision energies above about 0.1 mK the quenching rates are well described by a classical Langevin model, but at lower energies a fully quantal treatment is essential. We find that for the low initial vibrational state considered here ($v = 1$), the ultracold quenching rates are *not* substantially suppressed for fermionic atoms. For both bosons and fermions, vibrational quenching is much faster than elastic scattering in the ultralow-temperature regime. This contrasts with the situation found experimentally for molecules formed via Feshbach resonances in very high vibrational states.

PACS numbers: 03.75.Ss,34.20.Mq,31.50.Bc,33.80.Ps

I. INTRODUCTION

Dilute gases of alkali-metal atoms are a rich source of novel physical phenomena. Bose-Einstein condensates (BECs) were first created in such gases in 1995 [1, 2, 3] and have been the subject of intense exploration ever since. Further possibilities were opened up by the achievement of Fermi degeneracy in 1999 [4]. Among the alkali-metal atoms, lithium [3, 5] and potassium [4, 6] have a special status because both bosonic and fermionic isotopes are available and both Bose-Einstein condensation and Fermi degeneracy have been achieved. The present paper will focus on potassium.

In recent years, much interest has focussed on the interactions between atoms and the formation of molecules in ultracold gases. Donley *et al.* [7] showed that it is possible to form dimers of bosonic atoms such as ^{85}Rb by magnetic tuning from an atomic to a molecular state in the vicinity of a Feshbach resonance. However, molecules formed in this way in an atomic BEC proved to be short-lived (with lifetimes of milliseconds) because of atom-molecule and molecule-molecule collisions [7, 8, 9, 10]: the molecules are formed in the highest vibrational state that exists in the two-body potential well, and any collision that changes the vibrational state releases enough energy to eject both collision partners from the trap.

In summer 2003, Regal *et al.* [11] succeeded in forming ultracold diatomic molecules in a Fermi-degenerate gas of ^{40}K atoms by ramping the magnetic field through a Feshbach resonance. Such molecules are composite bosons. However, these too turned out to be short-lived (lifetime < 1 ms). Finally, at the end of 2003, a long-lived molecular BEC was created using the same technique [12] with a different Feshbach resonance. Such condensates have also been formed from dimers of ^6Li [13, 14, 15].

The use of fermionic isotopes appears to be crucial for the production of long-lived molecular condensates. The inelastic collisions that cause trap loss for molecules formed from bosonic atoms are sometimes suppressed for molecules formed from fermionic atoms [16, 17, 18, 19]. At magnetic fields where the atom-atom scattering length is large and positive ($a > 1000$ a_0), molecular lifetimes longer than 100 ms can be achieved. Petrov *et al.* [20] have explained the difference in collisional properties of dimers formed from bosonic and fermionic atoms in terms of the symmetries of the allowed wavefunctions. However, their derivation applies only to dimers in Feshbach resonance states and not to deeply bound molecular states.

In a previous study [21], we investigated ultralow energy collisions between spin-polarized Li atoms and Li_2 dimers, with the dimers in low-lying vibrational bound states. Our results showed no systematic differences in vibrational quenching between the bosonic ^7Li and fermionic ^6Li cases. This supports the conclusion that the suppression of inelastic collisions in the fermionic case requires *both* fermion symmetry [20] *and* the long-range nature of the molecules in Feshbach resonance states [22].

In the present paper, we study ultralow energy K + K_2 collisions involving three equivalent nuclei. We construct a new *ab initio* potential energy surface for the lowest spin-polarized electronic state of the potassium trimer ($1^4A_2'$) and investigate both bosonic (^{39}K, ^{41}K) and fermionic (^{40}K) cases. We perform quantum-mechanical scattering calculations at energies down to 1 nK. Elastic, inelastic and rearrangement processes are considered. Our quantum dynamical results show that, for all three systems, vibrational relaxation is more efficient than elastic scattering, as in our previous studies with ^{23}Na [23, 24] and $^{6,7}Li$ [21]. As in the case of lithium, there are no systematic differences in quenching rates for potassium dimers formed from bosonic and

fermionic atoms.

II. POTENTIAL ENERGY SURFACE OF $K_3(1^4A_2')$

We have carried out *ab initio* calculations on K_3 using a single-reference restricted open-shell variant [25] of the coupled-cluster method [26] with single, double and non-iterative triple excitations [RCCSD(T)]. We used the small-core ECP10MWB effective core potential (ECP) of Leininger *et al.* [27] together with the medium-sized valence basis sets of Soldán *et al.* [28]. The quasirelativistic [29] ECP treats the $1s^2$ electrons as core and the $3s^2$ $3p^6$ 4s electrons as valence. The valence basis set for K was used in uncontracted form. The resulting atomic polarizability (294.2 a_0^3) is in excellent agreement with the experimental value [30] (292.8 ± 6.1 a_0^3).

For interpolation purposes, the three-atom interaction potential was decomposed into a sum of additive and non-additive contributions,

$$V_{\rm trimer}(r_{12}, r_{23}, r_{13}) = \sum_{i<j} V_{\rm dimer}(r_{ij}) + V_3(r_{12}, r_{23}, r_{13}). \quad (1)$$

The full counterpoise correction of Boys and Bernardi [31] was employed to compensate for basis set superposition error in both dimer and trimer calculations. All the *ab initio* calculations were performed using the MOLPRO package [32].

The dimer interaction energy $V_{\rm dimer}(r)$ was first calculated on an irregular grid of 42 points at interatomic distances between 2.1 Å and 14.0 Å. The potential energy curve was generated using the modified 1D reciprocal-power reproducing kernel Hilbert space (RP-RKHS) interpolation method [33, 34]. The interpolation was done with respect to r^2 using RP-RKHS parameters $m = 2$ and $n = 3$. Beyond 14 Å the potential energy curve was thus extrapolated to the form

$$V_{\rm dimer}(r) = -\frac{C_6}{r^6} - \frac{C_8}{r^8} - \frac{C_{10}}{r^{10}}. \quad (2)$$

The long-range coefficients C_6 and C_8 were kept fixed to the published values of 3.897×10^3 $E_h a_0^6$ and 4.2×10^5 $E_h a_0^8$ respectively [35, 36]. The value of the "free" long-range coefficient C_{10} was then determined from the corresponding RP-RKHS coefficients [37], and was found to be 2.0243×10^{10} $E_h\, a_0^{10}$, which compares very well with 2.0294×10^{10} $E_h\, a_0^{10}$ from Ref. 36. Values of $D_{\rm e} = 252.6$ cm^{-1} and $r_{\rm e} = 5.79$ Å calculated from the resulting curve are also in good agreement with experimental results on $^{39}K_2$ ($D_{\rm e} = 252.74 \pm 0.12$ cm^{-1}, $r_{\rm e} = 5.7725(20)$ Å [38, 39]).

For quantum dynamics calculations, it is very important to have a potential energy function that can be interpolated smoothly (and without oscillations) between

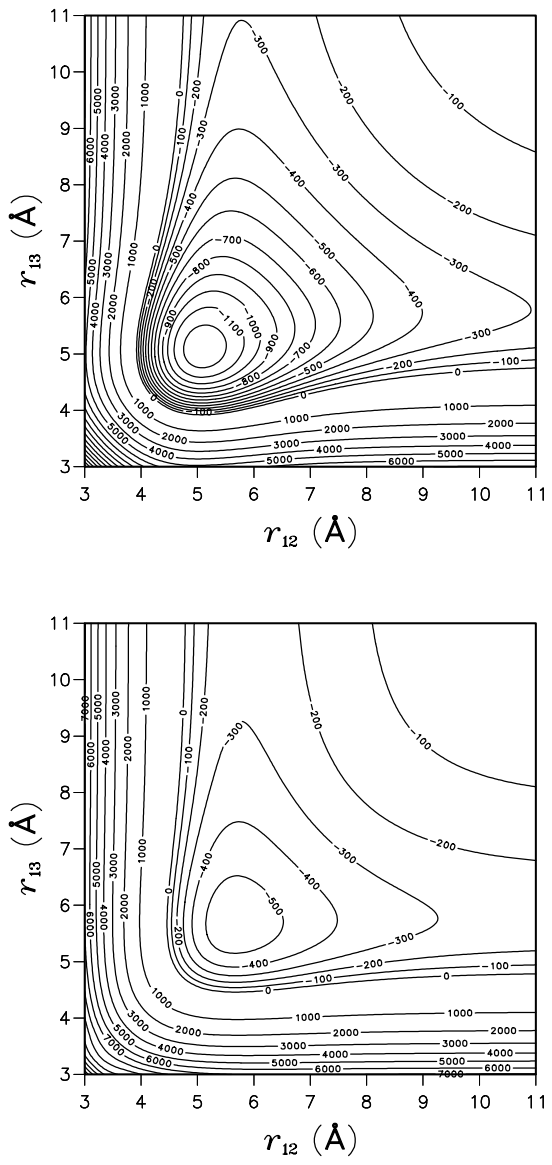

FIG. 1: Cuts through the K_3 quartet surface in valence coordinates. Upper panel: cut for a bond angle of 60°, showing the global minimum at -1269 cm^{-1} and 5.09 Å. Lower panel: cut at collinear geometries; the collinear minimum is at -565 cm^{-1} and 5.68 Å. Contours are labelled in cm^{-1}.

ab initio points. Oscillations often arise in low-energy regions if one or more points have much higher energies than those surrounding them. Some experimentation was needed to find a coordinate system in which interpolation could be carried out without problems. Jacobi and bond angle / bond length coordinates were rejected because they do not lend themselves to symmetrization, and hyperspherical coordinates proved unsuitable because some combinations of grid points pro-

duce geometries with atoms very close together and correspondingly high energies. In the end, we chose to calculate the potential grid in pure bond length coordinates (r_{12}, r_{23}, r_{31}). This has the advantage that points that are related by symmetry have coordinates that are also simply related.

The trimer interaction energy $V_{\rm trimer}$ was calculated at 325 points on a 3D grid covering the range of interatomic distances from 3.5 Å to 10.5 Å with step 0.5 Å. To avoid duplication, only points with $r_{12} \le r_{13} \le r_{23}$ are required. To meet geometrical constraints, all grid points must satisfy the triangular inequality $|r_{12} - r_{13}| \le r_{23} \le r_{12} + r_{13}$. The distance r_{23} was permitted to extend beyond 10.5 Å. The final grid consisted of 205 C_{2v} points, including 15 D_{3h} points and 120 $C_{\infty v}$ points; the latter include 15 $D_{\infty h}$ points. Each calculation was carried out using the full symmetry allowed by MOLPRO. The non-additive energies V_3 were extracted from the trimer interaction energies using Eq. (1).

For low-energy scattering calculations it is important to have an interaction potential that behaves correctly at long range. The RP-RKHS interpolation procedure in 1 dimension allows this as decribed above. However, multidimensional RP-RKHS interpolation always gives a potential that extrapolates beyond the points as a simple product of inverse powers in the different coordinates. The leading long-range terms in the non-additive energy are the third-order dipole-dipole-dipole (DDD) [40] and dipole-dipole-quadrupole (DDQ) [41] terms given by

$$V_3^{\rm DDD} = 3Z_{111}^{(3)} \frac{1 + 3\cos\phi_3 \cos\phi_1 \cos\phi_2}{r_{12}^3 r_{23}^3 r_{13}^3} \tag{3}$$

and

$$V_3^{\rm DDQ} = Z_{112}^{(3)} \left(W^{123} + W^{231} + W^{312}\right) \tag{4}$$

where

$$W^{ijk} = \frac{3}{16 r_{jk}^4 r_{ik}^4 r_{ij}^3} \left[9\cos\phi_k - 25\cos 3\phi_k + 6\cos(\phi_i - \phi_j) \times (3 + 5\cos 2\phi_k)\right] \tag{5}$$

and ϕ_i is the bond angle at atom i. It may be noted that the DDD term vanishes on a seam in the angular space and the DDQ term vanishes at all linear geometry configurations. Damped versions of these terms were therefore subtracted from the total non-additive energy V_3 before interpolation to give a quantity V_3',

$$V_3' = V_3 - f_{\rm damp}[V_3^{\rm DDD} + V_3^{\rm DDQ}]. \tag{6}$$

The coefficients $Z_{111}^{(3)}$ and $Z_{112}^{(3)}$ were taken to be $2.72 \times 10^5\ E_h\, a_0^9$ and $5.11 \times 10^6\ E_h\, a_0^{11}$ respectively [42]. The damping function serves to prevent the non-additive energy exploding at short range, and was chosen to have a product form, $f_{\rm damp}(r_{12}, r_{23}, r_{13}) = f(r_{12})\, f(r_{23})\, f(r_{13})$, where

$$f(r) = \exp\left[-(k_3/r - 1)^2\right] \qquad 0 < r < k_3 \tag{7}$$

$$= 1 \qquad r \ge k_3 \tag{8}$$

with the cut-off parameter $k_3 = 8.0$ Å.

The leading term of the multipole asymptotic expansion of V_3' is the fourth-order dipole-dipole-dipole term (DDDD), which has a more complicated (unfactorizable) form [43],

$$V_3^{\rm DDDD} = -\frac{45}{64} Z_{1111}^{(3)} \left[\frac{1 + \cos^2\phi_1}{r_{12}^6 r_{13}^6} + \frac{1 + \cos^2\phi_2}{r_{12}^6 r_{23}^6} + \frac{1 + \cos^2\phi_3}{r_{13}^6 r_{23}^6}\right]. \tag{9}$$

The coefficient $Z_{1111}^{(3)}$ is not yet known, so this term cannot be subtracted out. However, the term is negative at all geometries, so it can be eliminated by defining $V_3'' = g \times V_3'$, where

$$g = \frac{r_{12}^3 r_{23}^3 r_{13}^3}{(1 + \cos^2\phi_1)\, r_{23}^6 + (1 + \cos^2\phi_2)\, r_{13}^6 + (1 + \cos^2\phi_3)\, r_{12}^6}. \tag{10}$$

The leading asymptotic term of the function V_3'' now has the form $-$constant $\times\ r_{12}^{-3} r_{23}^{-3} r_{13}^{-3}$ and is suitable for an "isotropic" extrapolation of the type that results from a multidimensional RP-RKHS interpolation. The function V_3'' was interpolated using the fully symmetrized 3D RP-RKHS interpolation method [44]. The interpolation was

done with respect to the reduced coordinate $(r/S)^3$ and with parameters $S = 10.0$ Å, $m = 0$, $n = 2$ in each interatomic distance. The original potential is then rebuilt as

$$V_3 = \frac{1}{g} V_3'' + f_{\rm damp} \left[V_3^{\rm DDD} + V_3^{\rm DDQ} \right]. \qquad (11)$$

The final potential for quartet K_3, $V_{\rm trimer}$, has a global minimum at -1269 cm^{-1} at an equilateral (D_{3h}) geometry $r_{12} = r_{13} = r_{23} = 5.09$ Å. There is a shallow secondary minimum at -565 cm^{-1} at a linear $D_{\infty h}$ geometry with $r_{12} = r_{13} = 5.68$ Å. Two cuts through the surface are shown as contour plots in Fig. 1 for values of the valence angle 60° and 180°.

III. QUANTUM SCATTERING THEORY

A. Method

We have performed three-dimensional quantum dynamical calculations for K + K_2 including reactive scattering for total angular momenta $J = 0 - 5$. A time-independent formalism (which is the most appropriate choice for ultralow energy scattering) was used. The configuration space is divided into an inner and an outer region depending on the atom–diatom distance. In the inner region, typically for hyperradius smaller than $\rho_{\rm max}$ = 60 a_0, we use a formalism based on body-frame democratic hyperspherical coordinates [45, 46] which has previously proved successful in describing atom-diatom insertion reactions such as $N(^2D) + H_2 \rightarrow NH + H$ [47, 48] and $O(^1D) + H_2 \rightarrow OH + H$ [49, 50]. These coordinates were also used in our recent work on Na + Na_2 [23, 24] and Li + Li_2 [21].

At each hyperradius ρ, we determine a set of eigenfunctions of a fixed-hyperradius reference hamiltonian $H_0 = T + V$ by expanding the wavefunction in a set of pseudohyperspherical harmonics. The reference hamiltonian incorporates the kinetic energy T arising from deformation and rotation around the axis of least inertia and the potential energy V. A typical set of eigenvalues for K_3 is shown in Fig. **??**. At small hyperradius, the adiabatic states in each sector span a large fraction of configuration space and allow for atom exchange. The scattering wave function is expanded on this set of hyperspherical adiabatic states. This yields a set of close-coupling equations, which are solved using the Johnson–Manolopoulos log-derivative propagator [51].

In the outer region, we use the standard Arthurs-Dalgarno formalism [52] based on Jacobi coordinates and assume that the atom–molecule interaction can be described by an isotropic potential $U(R)$. We thus assume that no inelastic scattering occurs in the outer region. The radial channel wavefunctions in this region are solutions of the equation (in atomic units)

$$\Big(-\frac{1}{2\mu}\frac{d^2}{dR^2} + \frac{l(l+1)}{2\mu R^2} + U(R)\Big) F(R) = \frac{k^2}{2\mu} F(R), \quad (12)$$

where μ is the K–K_2 reduced mass and k and l are respectively the channel wavenumber and the orbital angular momentum quantum number. The potential $U(R)$ behaves asymptotically as $-C_{\rm K-K_2}/R^6$ with a coefficient $C_{\rm K-K_2} = 9050\ E_h a_0^6$. Equation (12) is solved by a finite difference method in the range 60–10000 a_0. The matching of the inner and outer wavefunctions is performed on a boundary which is an hypersphere of radius $\rho = 60\ a_0$. This yields the reactance K, scattering S and transition T matrices.

B. Cross sections and Wigner laws

At ultralow energies, for *both* bosonic and fermionic systems, only T_{ii} elements with a relative atom–diatom orbital angular momentum $l = 0$ contribute. We obtain elastic and quenching cross sections from the diagonal elements T_{ii} of the transition T matrix,

$$\sigma_E = \frac{\pi}{k^2}|T_{ii}|^2; \qquad \sigma_Q = \frac{\pi}{k^2}(1 - |1 - T_{ii}|^2). \qquad (13)$$

The complex scattering length can be written as

$$a = \frac{1}{2i} \lim_{k\to 0} \Big(\frac{T_{ii}}{k} \Big). \qquad (14)$$

The elastic and quenching cross sections at threshold can therefore be written respectively in terms of the square modulus of the scattering length and the imaginary part of the scattering length,

$$\sigma_E = 4\pi|a|^2; \qquad \sigma_Q = -\frac{4\pi}{k} Im(a). \qquad (15)$$

The elastic and quenching rate coefficients K_E and K_Q are obtained by multiplying the cross sections by the atom–diatom relative velocity, k/μ in atomic units,

$$K_E = \frac{4\pi|a|^2}{\mu} k; \qquad K_Q = -\frac{4\pi}{\mu} Im(a). \qquad (16)$$

At ultralow collision energy, where only $l = 0$ is involved, the elastic rate coefficient vanishes as the collision energy decreases and the quenching rate coefficient becomes constant.

The Wigner threshold laws [53] for an orbital angular momentum l give the following dependences on the collision energy for partial elastic and quenching cross sections,

$$\sigma_E^l \sim E_{\rm coll}^{2l}; \qquad \sigma_Q^l \sim E_{\rm coll}^{l-1/2}. \qquad (17)$$

The energy-dependence for partial elastic and quenching rate coefficients is obtained by multiplying these cross sections by $(2E_{\rm coll}/\mu)^{1/2}$,

$$K_E^l \sim E_{\rm coll}^{2l+1/2}; \qquad K_Q^l \sim E_{\rm coll}^{l}. \qquad (18)$$

We also need state-to-state cross sections for the calculation of rotational distributions. For partial wave J, they are generated from the T matrix using the standard formula,

$$\sigma_{vj\to v'j'} = \frac{\pi}{(2j+1)k_{vj}^2}\sum_{J=0}^{\infty}(2J+1)\sum_{l=|J-j|}^{J+j}\sum_{l'=|J-j'|}^{J+j'}|T^J_{v'j'l',vjl}|^2. \quad (19)$$

In this paper, we present for the first time differential cross sections (DCS) for an atom-diatom system at ultralow collision energy. The state-to-state magnetically averaged DCS is given by

$$\frac{d\sigma_{vj\to v'j'}}{d\omega} = \frac{1}{4k_{vj}^2(2j+1)}\sum_{m,m'}\left|\sum_J(2J+1)d^J_{m',m}(\theta_{\rm cm})T^J_{v'j'm',vjm}\right|^2 \quad (20)$$

where $d^J_{m',m}$ is a Wigner reduced rotation matrix element.

In Eq. (20), $\theta_{\rm cm}$ is the scattering angle in the center-of-mass (CM) coordinate system. $\theta_{\rm cm} = 0°$ is defined as the direction of the CM velocity vector of initial K atoms and corresponds to forward scattering for the K products (and backward scattering for the K_2 products). Backward scattering of the K products (forward scattering for the K_2 products) thus corresponds to $\theta_{\rm cm} = 180°$.

C. Symmetries

We are interested in elastic scattering and vibrational relaxation, which have different roles in the formation and stability of a molecular BEC. Elastic collisions are favorable for evaporative cooling towards condensation, whereas inelastic collisions provide a trap loss mechanism. For evaporative cooling, knowledge of the ratio of elastic to non-elastic rate coefficients is crucial.

Here the system is composed of three indistinguishable atoms ^{39}K, ^{40}K or ^{41}K and the K_3 potential energy surface is barrierless. We thus have to take into account two different collisional processes: elastic collision K + $K_2(v,j)$, and vibrational relaxation K + $K_2(v,j) \to$ K + $K_2(v',j')$. For this latter process, the rovibrational energy $E_{v',j'}$ of the product molecule is smaller than that of the initial molecule.

We consider three atoms K in their stretched spin states, with $F = F_{\rm max} = S + I$ and $M_F = F$. For $S = 1/2$, this requires $M_S = +1/2$ and so the electronic spin wavefunction is symmetric with respect to exchange of nuclei. ^{39}K and ^{41}K atoms have $I = 3/2$, so $M_I = +3/2$ in the spin-stretched state and the nuclear spin wavefunction is also symmetric. Since the total spin F is an integer, these atoms are composite bosons. For ^{40}K, $I = 4$ so that F is half-integer and the atoms are composite fermions. For the spin-stretched state of ^{40}K, $F = F_{\rm max} = I + S = 9/2$ and $M_F = M_{\rm max} = +9/2$. In this work, all magnetic interactions are neglected, so that the electronic and nuclear spin orientations are unchanged during the collision.

The spatial part of the *electronic* wavefunction for the $1^4A_2'$ state is antisymmetric with respect to exchange of nuclei. As a consequence, for ^{39}K or ^{41}K the spatial part of the nuclear wavefunction has to be symmetric, whereas for ^{40}K it has to be antisymmetric. In our quantum scattering code, this is achieved by selecting pseudohyperspherical harmonics in the basis sets for bosons and fermions to give the correct symmetry for the nuclear wavefunction. The adiabatic states in each sector are obtained by a variational expansion on a basis of hyperspherical harmonics with A_1 symmetry (of the complete nuclear permutation group S_3) for bosons and A_2 symmetry for fermions. They are respectively fully symmetric and fully antisymmetric with respect to particle permutations to account for the indistinguishability of atoms.

D. Partial waves

The behavior at the lowest collision energies is more subtle in the molecular case than in the atomic case. In atom-atom collisions, the fundamental difference between bosons and fermions is seen in the behaviour of cross sections. For two identical spin-polarized bosons, the elastic cross section becomes constant as the collision energy goes to zero because only the s-wave ($l = 0$) contributes. In contrast, for two fermions, the elastic cross section decreases as the collision energy decreases because there is no s-wave and only the p-wave ($l = 1$) contributes at ultralow energy.

In atom-molecule collisions, by contrast, $l = 0$ is allowed for *both* bosons and fermions. For three identical atoms, only one partial wave is involved at ultralow energy: $J = 0^+$ for bosons and $J = 1^-$ for fermions. These both include $l = 0$.

The channels contributing to each partial wave J^Π up to $J = 3$ are shown for bosons in Table I. The total mechanical angular momentum $\mathbf{J = j + l}$ is the vector sum of the diatomic rotational angular momentum $\mathbf{j}$ and the orbital angular momentum $\mathbf{l}$. In this study, we consider initial $^{39}K_2$ or $^{41}K_2$ molecules initially in rovibrational state ($v = 1, j = 0$), so the parity Π is $(-1)^{j+l} = (-1)^l = (-1)^J$. For $^{40}K_2$, only odd j is allowed so we consider the initial state ($v = 1, j = 1$). The partial waves for fermions (with contributing chan-

TABLE I: Channels contributing to partial waves J^Π, showing allowed values of the orbital angular momentum l for a rovibrational state $(v, j = 0)$ of $^{39}K_2$ or $^{41}K_2$ molecules formed from bosonic atoms.

0^+	1^-	2^+	3^-
$l = 0$	$l = 1$	$l = 2$	$l = 3$

TABLE II: Channels contributing to partial waves J^Π, showing allowed values of the orbital angular momentum l for a rovibrational state $(v, j = 1)$ of a $^{40}K_2$ molecule formed from fermionic atoms.

0^+	1^-	2^+	3^-
$l = 1$	$l = 0, 2$	$l = 1, 3$	$l = 2, 4$
	1^+	2^-	3^+
	$l = 1$	$l = 2$	$l = 3$

nels shown in Table II) can be separated into two categories depending on the lowest value of l (or Ω, which is the projection of the total angular momentum J onto the axis of least inertia in the corresponding hyperspherical basis set). The parity-favored partial waves include $\Omega = 0$ and the parity is the same as for the boson case. In contrast, for the parity-unfavored partial waves the $\Omega = 0$ component is forbidden (as is the lowest value of l) and the lowest value of Ω is 1. The parity-favored and unfavored partial waves have parity $(-1)^J$ and $(-1)^{J+1}$ respectively.

E. Convergence and computer requirements

$K + K_2$ collisions are the most difficult and demanding ever studied in quantum dynamics calculations, because all three atoms are heavy and the potential well is deep. Careful attention has been devoted to the convergence of the calculations. There are three crucial parameters for convergence: the sizes of the basis sets, the size of each sector and the asymptotic matching distance.

First, the number of fixed-ρ eigenstates included in solving the coupled equations in each sector must be large enough for convergence. It is essential to include many closed channels. For both bosonic and fermionic systems, this number, which is also the number of coupled equations, increases about from 250 for $J = 0$ to 1411 for $J = 5$. The time taken to solve the coupled equations varies respectively from 2 minutes to 4 hours per collision energy on a Power4 P690 IBM computer. The fixed-ρ eigenstates are expanded in a pseudo-hyperspherical harmonic basis built from trigonometric functions, truncated at $\Lambda_{\max}$, the maximum value of the grand angular momentum. $\Lambda_{\max}$ varies from 198 (867 harmonics) at small hyperradius to 558 (6625 harmonics) at large hyperradius. The calculation to build the basis sets takes 180 hours and produces an output binary file of 40 Gigabytes which contains all information for the close-coupling code.

Secondly, the size of each sector must be small enough to give converged results. For both bosons and fermions, two different sector sizes were used: 0.025 a_0 from $\rho = 8.0$ to 26.0 a_0 and 0.05 a_0 from 26 a_0 to the matching distance 60 a_0. This yields 1400 sectors, which is about 4 times larger than were used for the case of Na_3 [23, 24].

Thirdly, the matching distance $\rho_{\max}$, where the adiabatic states are projected onto the arrangement channels, must be chosen to describe correctly K_2 molecules in the vibrational states required (in even j states for bosons and odd j states for fermions). We have taken $\rho_{\max} = 60$ a_0, which is larger than the value of 50 a_0 for the Na_3 case. For bosons, the hyperspherical wavefunction was projected onto a set of $^{39}K_2$ or $^{41}K_2$ rovibrational functions with $j_{\max} = (76, 70, 66, 60, 56, 50, 42, 34, 24, 2)$ for $v = 0, \ldots, 9$. For fermions $^{40}K_2$, rovibrational functions with $j_{\max} = (77, 71, 67, 61, 55, 49, 43, 35, 25, 7)$ were used.

At collision energies below 1 μK, only the partial wave that includes $l = 0$ contributes to cross sections ($J = 0^+$ for bosons and $J = 1^-$ for fermions). However at higher energies, other partial waves contribute. In this work, for the bosonic cases we have converged the elastic and quenching cross sections for collision energies up to 10 mK by including partial waves up to $J = 5$. Calculations for the fermionic system $^{40}K + {}^{40}K_2$ are converged up to 100 μK by including partial waves up to $J = 2$. We have considered only three values of J for fermions because the calculations are twice as expensive for fermions as for bosons (because both parity-favored and parity-unfavored partial waves contribute in the fermion case).

IV. DYNAMICAL RESULTS AND DISCUSSION

The following discussion refers to collisions involving ^{39}K bosons unless otherwise stated.

A. Hyperspherical adiabatic energies

The hyperspherical adiabatic energies for the lowest 250 hyperspherical states with $\Omega = 0$ are shown as a function of the hyperradius ρ in Fig. **??** (not shown here because the eps file is too big). If we consider $^{39}K_2$ molecules in their $(v = 1, j = 0)$ rovibrational state, we have 15 hyperspherical states asymptotically open, and 235 asymptotically closed. There are two minima: the deepest corresponds to the equilateral geometry, while the secondary minimum at around 20 a_0 corresponds to the linear geometry. At large ρ, the hyperspherical adiabatic energies tend to the energies of the diatomic molecule K_2. The zero of energy is taken as the dissociation limit to three atoms.

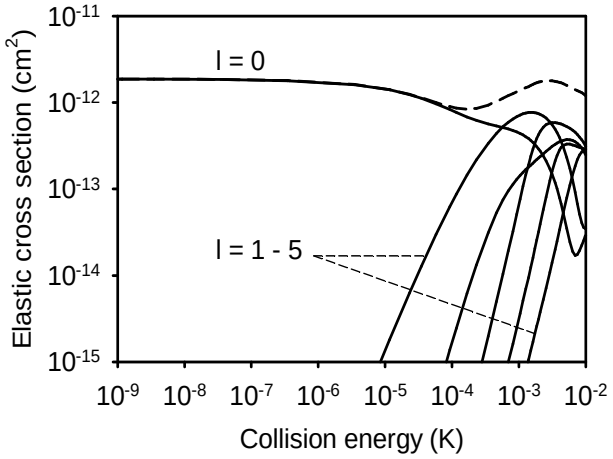

FIG. 2: Elastic cross sections for ^{39}K + ^{39}K$_2$($v = 1, j = 0$): partial as solid lines, total as dashed line.

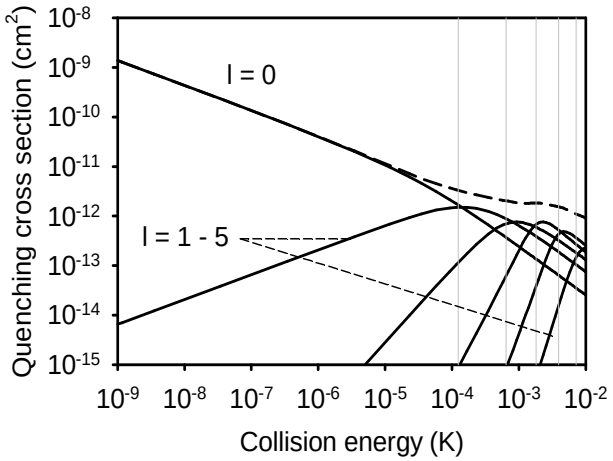

FIG. 3: Quenching cross sections for ^{39}K + ^{39}K$_2$($v = 1, j = 0$): partial as solid lines, total as dashed line. Vertical lines correspond to the maxima of the effective potential (see text for detail).

B. Cross sections and rate coefficients

The fully converged elastic and quenching integral cross sections and their partial wave contributions for $l = 0$ to 5 are shown in Figs. 2 and 3 for collision energies between 1 nK and 10 mK. At $E_{\rm coll} = 10^{-9}$ K, the elastic cross section is about 1.9×10^{-12} cm^2 whereas the quenching cross section is about 1.4×10^{-9} cm^2. The slope of each partial cross section is given by the Wigner laws (Eq. (17)) at ultralow energy except for the case of elastic scattering for $l > 1$, where the dispersion-modified threshold law $\sigma_E^l \sim E_{\rm coll}^3$ applies. The upper limit of the Wigner regime is 0.1 μK. The minimum in the $l = 0$ partial elastic cross section near 10^{-2} K arises simply from a near-zero phase-shift in the formula for the elastic cross section.

The quenching cross section for a partial wave with $l >$

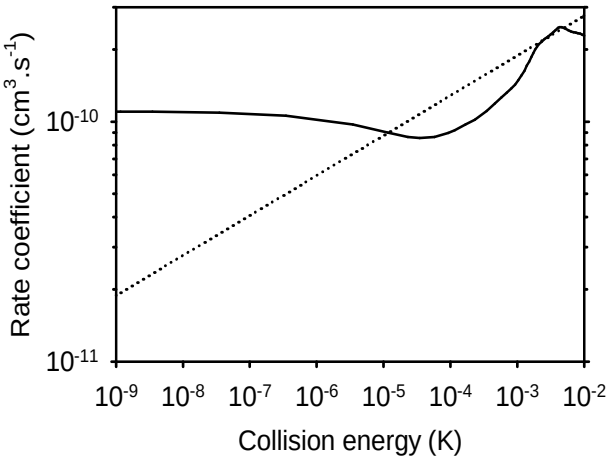

FIG. 4: Total quenching rate coefficients for ^{39}K + ^{39}K$_2$($v = 1, j = 0$). The result from the Langevin model is shown as a dotted line.

0 shows a maximum at a collision energy which is given approximately by the maximum of the effective potential including the centrifugal and dispersion terms,

$$V^l(R) = \frac{l(l+1)}{2\mu R^2} - \frac{C_{\rm K-K_2}}{R^6}. \qquad (21)$$

The height of the barrier is

$$V^l_{\rm max} = \frac{[l(l+1)]^{3/2}}{3\mu^{3/2}(6C_{\rm K-K_2})^{1/2}} \qquad (22)$$

at a distance

$$R^l_{\rm max} = \left[\frac{6\mu C_{\rm K-K_2}}{l(l+1)}\right]^{1/4}. \qquad (23)$$

The resulting barrier heights are included in Fig. 3. The first vertical line corresponds to the $l = 1$ partial wave and so on up to the $l = 5$ partial wave. It may be seen that each partial wave has a maximum at an energy slightly higher than the corresponding $V^l_{\rm max}$. At collision energies below the centrifugal barrier, the quenching partial cross sections for each l follow Wigner laws given by Eq. (17). Above the centrifugal barrier, the quenching probabilities come close to their maximum value of 1 and the cross sections vary as E^{-1} because of the k^{-2} factor in the expression for the cross section.

The total quenching rate coefficient is larger than the elastic rate over a wide range of collision energies, up to 1 mK, and is three orders of magnitude larger than the elastic rate at 1 nK (Fig. 8). The large quenching rates are consistent with recent experiments that create molecules in atomic Bose-Einstein condensates by Feshbach resonance tuning [7, 8, 9, 10]; for bosonic atoms, such experiments were unable to produce a long-lived molecular condensate because of the efficiency of quenching collisions.

At high collision energy, when several partial waves are involved ($l = 0 - 5$), the total quenching rate coefficient can be compared with that given by the classical Langevin capture model [54],

$$K_Q^{\rm capture}(E) = \frac{3\pi}{2^{1/6}} \left(\frac{C^{1/3}_{\rm K-K_2}}{\mu^{1/2}} \right) E^{1/6} \qquad (24)$$

This rate coefficient is shown as a function of collision energy in Fig. 4. It may be seen that there is semi-quantitative agreement between our quantum results and the capture model for collision energies above 0.1 mK. Below that energy, differences appear because there are fewer partial waves and the dynamics must then be described by a full quantum-mechanical treatment.

C. Differential cross sections

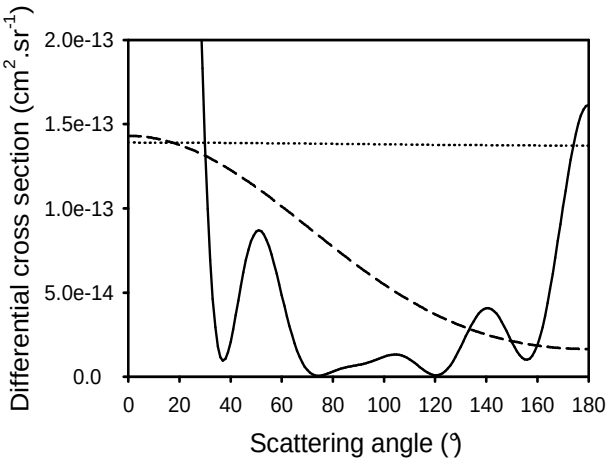

FIG. 5: Differential cross section for elastic scattering at 10^{-6} K (dotted line), 10^{-4} K (dashed line) and 10^{-2} K (solid line). The large forward scattering at 10^{-2} K is not completely shown; at zero degree the DCS value is 3×10^{-12} cm^{2}sr^{-1}.

Total differential cross sections (Eq. (20)) for elastic and quenching processes with $^{39}K_2$ molecules initially in ($v = 1, j = 0$) are shown in Figs. 5 and 6 for collision energies 10^{-6} K, 10^{-4} K and 10^{-2} K. At 10^{-6} K, where only the $l = 0$ and 1 partial waves contribute, the elastic and quenching DCS are quasi-isotropic. Below this energy (not shown), only the $l = 0$ partial wave is involved and so the DCS are fully isotropic. At higher energies, other partial waves contribute and the DCS depend on the center-of-mass scattering angle $\theta_{\rm cm}$.

For the elastic process, Figure 5 shows that backward scattering is smaller at 10^{-4} K than at 10^{-6} K, whereas forward scattering is similar. At 10^{-2} K, an enhancement of forward scattering is found. Undulations at this energy are simply due to a rainbow effect.

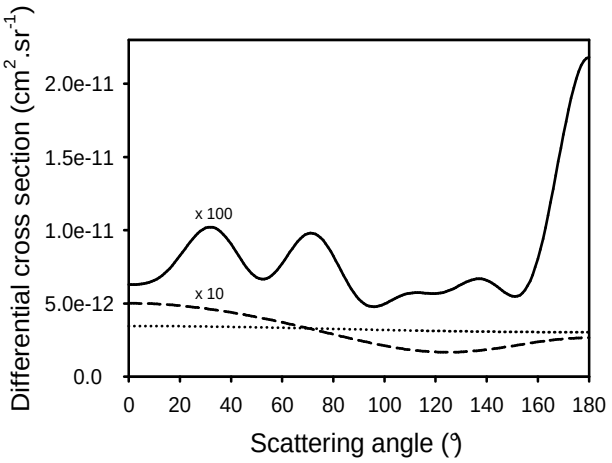

FIG. 6: Differential cross section for vibrational relaxation at 10^{-6} K (dotted line), 10^{-4} K (dashed line) and 10^{-2} K (solid line).

In contrast, the behavior of the quenching DCS is less systematic (Figure 6). The angular distribution is strongly peaked in the backward direction at 10^{-2} K whereas the forward scattering is dominant at 10^{-4} K. In addition, at 10^{-2} K the quenching DCS presents some oscillations in the sideways scattering with two pronounced maxima at 30 and 70 degrees.

D. Final rotational distributions

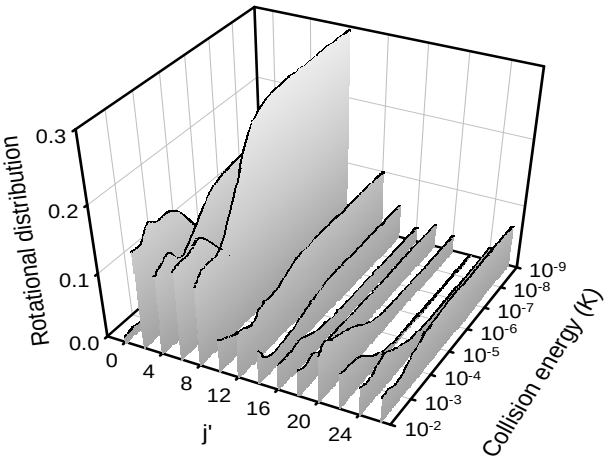

FIG. 7: Rotational distributions as a function of the collision energy. The label j' is the final rotational quantum number of $^{39}K_2(v' = 0)$.

The final rotational distribution for $^{39}K_2$ molecules initially in ($v = 1, j = 0$) is shown in Fig. 7 as a function of the collision energy. At each energy, we have divided each rotationally-resolved cross section (corresponding to a given final rotational quantum number j'

for $^{39}K_2(v' = 0)$) by the total quenching cross section. The sum of the distribution over j' gives unity at fixed energy. Because cross sections obey the Wigner laws (Eq. (17), the rotational distribution becomes constant in the ultracold regime. The final rotational state $j' = 8$ is the most populated at 1 nK whereas $j' = 2, 4, 6, 8$ are the most populated at 10 mK. Figure 7 also shows that only the lowest rotational states are significantly populated at all collision energies.

E. Bosons versus fermions

In Fig. 8 we compare the total elastic and quenching rate coefficients in the ultracold regime for the three systems: $^{39}K + {}^{39}K_2$ or $^{41}K + {}^{41}K_2$, composed of bosonic atoms and $^{40}K + {}^{40}K_2$, composed of fermionic atoms.

In the ultracold regime, the total rate coefficients are very similar for the two bosonic systems. However the rotationally state-resolved cross sections (not shown here) are different and the similarity of the total cross sections and rate coefficients is evidently coincidental. The rotational distributions are sensitive to the mass and also to the interaction potential as in $Na + Na_2$ [24].

Figure 8 shows that the quenching processes are very efficient even for the fermionic system. There is only a small difference between fermions and bosons. Both elastic and quenching rate coefficients are slightly smaller for the fermionic system than for the bosonic systems. However the ratio of elastic to quenching rate coefficients is nearly the same for bosons and fermions.

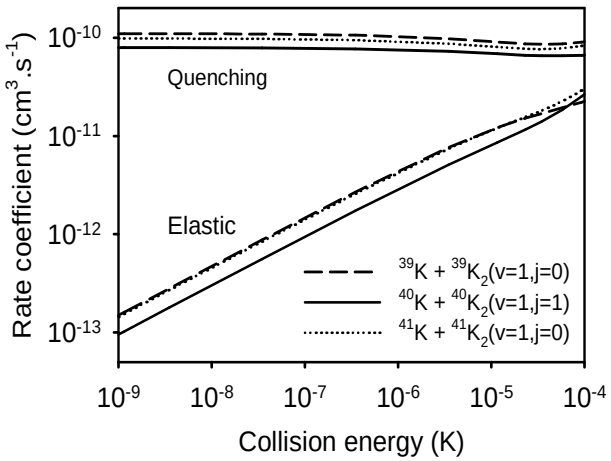

FIG. 8: Comparison of elastic and quenching rate coefficients for bosons (dashed and dotted lines) and fermions (solid line).

V. CONCLUSION

We have performed the first quantum dynamics calculations for $K + K_2$ collisions in the energy range 1 nK - 10 mK, using a new quartet potential energy surface for the potassium trimer. We have found that the quenching rate coefficient is much larger than the elastic rate coefficient at ultralow collision energies. This applies for all three collisions studied here, $^{39}K + {}^{39}K_2$, $^{41}K + {}^{41}K_2$, and $^{40}K + {}^{40}K_2$ where the initial K_2 molecules are in the $(v = 1, j = 0)$ rovibrational state for bosons or $(v = 1, j = 1)$ for fermions. Thus K_2 molecules in these states are not good candidates to accumulate large densities of ultracold molecules or to achieve long-lived molecular BEC. For the bosonic systems (^{39}K and ^{41}K), the results are qualitatively similar to those we obtained previously for ^{23}Na [23, 24] and ^{7}Li [21] atoms.

The quantum results for quenching rates agree semi-quantitatively with the Langevin model at high collision energies, but below 0.1 mK the dynamics is described only by the quantum theory.

The study of the fermionic system with ^{40}K atoms of particular interest, because it has recently been possible to create stable molecular BECs of $^{6}Li_2$ and $^{40}K_2$ [12, 13, 14, 15]. In these experiments, molecules were formed in the highest vibrational state supported by the potential well and it was found that inelastic collisions were suppressed by Pauli blocking [20]. Our result shows that for $^{40}K_2$ molecules in the initial vibrational states $v = 1$, there is no suppression of the quenching process.

Calculations with potassium atoms in higher vibrational states for both bosonic and fermionic systems are in progress. Future studies involving mixed collisions, i.e. with two different isotopes of potassium, are also planned.

ACKNOWLEDGMENTS

The dynamical calculations reported in this paper were performed with computer time provided by the "Institut du Développement des Ressources en Informatique Scientifique" (IDRIS, Orsay) and by the "Pôle de Calcul Intensif de l'Ouest" (PCIO, Rennes). PS and JMH are grateful to EPSRC for support under research grant no. GR/R17522/01.

[1] M. H. Anderson, J. R. Ensher, M. R. Matthews, C. E. Wieman, and E. A. Cornell, Science **269**, 198 (1995).

[2] K. B. Davis, M. Mewes, M. R. Andrews, N. J. van Druten, D. S. Durfee, D. M. Kurn, and W. Ketterle, Phys. Rev. Lett. **75**, 3969 (1995).

[3] C. C. Bradley, C. A. Sackett, J. J. Tollett, and R. G. Hulet, Phys. Rev. Lett. **75**, 1687 (1995).

[4] B. DeMarco and D. S. Jin, Science **285**, 1703 (1999).

[5] A. G. Truscott, K. E. Strecker, W. I. McAlexander, G. B. Partridge, and R. G. Hulet, Science **291**, 2570 (2001).

[6] G. Modugno, G. Ferrari, G. Roati, R. J. Brecha, A. Simoni, and M. Inguscio, Science **294**, 1320 (2001).

[7] E. A. Donley, N. R. Claussen, S. T. Thompson, and C. E. Wieman, Nature (London) **417**, 529 (2002).

[8] J. Herbig, T. Kraemer, M. Mark, T. Weber, C. Chin, H.-C. Nägerl, and R. Grimm, Science **301**, 1510 (2003).

[9] S. Dürr, T. Volz, A. Marte, and G. Rempe, Phys. Rev. Lett. **92**, 020406 (2004).

[10] T. Mukaiyama, J. R. Abo-Shaeer, K. Xu, J. K. Chin, and W. Ketterle, Phys. Rev. Lett. **92**, 180402 (2004).

[11] C. A. Regal, C. Ticknor, J. L. Bohn, and D. S. Jin, Nature (London) **424**, 47 (2003).

[12] M. Greiner, C. A. Regal, and D. S. Jin, Nature (London) **426**, 537 (2003).

[13] S. Jochim, M. Bartenstein, A. Altmeyer, G. Hendl, S. Riedl, C. Chin, J. Hecker Denschlag, and R. Grimm, Science **302**, 2101 (2003).

[14] M. W. Zwierlein, C. A. Stan, C. H. Schunck, S. M. F. Raupach, S. Gupta, Z. Hadzibabic, and W. Ketterle, Phys. Rev. Lett. **91**, 250401 (2003).

[15] T. Bourdel, L. Khaykovich, J. Cubizolles, J. Zhang, F. Chevy, M. Teichmann, L. Tarruell, S. J. J. M. F. Kokkelmans, and C. Salomon Phys. Rev. Lett. **93**, 050401 (2004).

[16] C. A. Regal, M. Greiner, and D. S. Jin, Phys. Rev. Lett. **92**, 083201 (2004).

[17] K. E. Strecker, G. B. Partridge, and R. G. Hulet, Phys. Rev. Lett. **91**, 080406 (2003).

[18] J. Cubizolles, T. Bourdel, S. J. J. M. F. Kokkelmans, G. V. Shlyapnikov, and C. Salomon, Phys. Rev. Lett. **91**, 240401 (2003).

[19] S. Jochim, M. Bartenstein, A. Altmeyer, G. Hendl, C. Chin, J. Hecker Denschlag, and R. Grimm, Phys. Rev. Lett. **91**, 240402 (2003).

[20] D. S. Petrov, C. Salomon, and G. V. Shlyapnikov, Phys. Rev. Lett. **93**, 090404 (2004).

[21] M. T. Cvitaš, P. Soldán, J. M. Hutson, P. Honvault, and J.-M. Launay, `arXiv: cond-mat/0409709`; submitted to Phys. Rev. Lett. (2004).

[22] T. Köhler, T. Gasenzer, P. S. Julienne, and K. Burnett, Phys. Rev. Lett. **91**, 230401 (2003).

[23] P. Soldán, M. T. Cvitaš, J. M. Hutson, P. Honvault, and J.-M. Launay, Phys. Rev. Lett. **89**, 153201 (2002).

[24] G. Quéméner, P. Honvault, and J.-M. Launay, Eur. Phys. J. D **30**, 201 (2004).

[25] P. J. Knowles, C. Hampel, and H.-J. Werner, J. Chem. Phys. **99**, 5219 (1993); erratum J. Chem. Phys. **112**, 3106 (2000).

[26] J. Čížek, J. Chem. Phys. **45**, 4526 (1966).

[27] T. Leininger, A. Niclass, V. Küchle, H. Stoll, M. Dolg, and A. Bergner, Chem. Phys. Lett. **255**, 274 (1996).

[28] P. Soldán, M. T. Cvitaš, and J. M. Hutson, Phys. Rev. A **67**, 054702 (2003).

[29] J. J. Wood and A. M. Boring, Phys. Rev. B **18**, 2701 (1978).

[30] R. W. Molof, H. L. Schwartz, T. M. Miller, and B. Bederson, Phys. Rev. A **10**, 1131 (1974).

[31] S. F. Boys and F. Bernardi, Mol. Phys. **19**, 553 (1970).

[32] MOLPRO is a package of *ab initio* programs written by H.-J. Werner and P. J. Knowles with contributions from others; for more information see the www page http://www.tc.bham.ac.uk/molpro/.

[33] T-S. Ho and H. Rabitz, J. Chem. Phys. **104**, 2584 (1996).

[34] T-S. Ho and H. Rabitz, J. Chem. Phys. **113**, 3960 (2000).

[35] A. Derevianko, W. R. Johnson, M. S. Safronova, and J. F. Babb, Phys. Rev. Lett. **82**, 3589 (1999).

[36] S. G. Porsev and A. Derevianko, J. Chem. Phys. **119**, 844 (2003).

[37] P. Soldán and J. M. Hutson, J. Chem. Phys. **112**, 4415 (2000).

[38] L. Li, A. M. Lyyra, W. T. Luh, and W. C. Stwalley, J. Chem. Phys. **93**, 8452 (1990).

[39] G. Zhao, W. T. Zemke, J. T. Kim, Bing Ji, H. Wang, J. T. Bahns, W. C. Stwalley, L. Li, A. M. Lyyra, and C. Amiot, J. Chem. Phys. **105**, 7976 (1996).

[40] B. M. Axilrod and E. Teller, J. Chem. Phys. **11**, 299 (1943); Y. Muto, Proc. Phys. Math. Soc. Japan **17**, 629 (1943).

[41] R. J. Bell, J. Phys. B: Atom. Molec. Phys. **3**, 751 (1970).

[42] S. H. Patil and K. T. Tang, J. Chem. Phys. **106**, 2298 (1997).

[43] W. L. Bade, J. Chem. Phys. **28**, 282 (1958).

[44] J. Higgins, T. Hollebeek, J. Reho, T.-S. Ho, K. K. Lehmann, H. Rabitz, G. Scoles, and M. Gutowski, J. Chem. Phys. **112**, 5751 (2000).

[45] J.-M. Launay and M. Le Dourneuf, Chem. Phys. Lett. **163**, 178 (1989).

[46] P. Honvault and J.-M. Launay, in *Theory of Chemical Reaction Dynamics*, edited by A. Lagana and G. Lendvay (NATO Science Series vol. 145, Kluwer, 2004), p. 187.

[47] P. Honvault and J.-M. Launay, J. Chem. Phys. **111**, 6665 (1999).

[48] N. Balucani, L. Cartechini, G. Capozza, E. Segoloni, P. Casavecchia, G.G. Volpi, F.J. Aoiz, L. Bañares, P. Honvault, and J.-M. Launay, Phys. Rev. Lett. **89**, 013201 (2002).

[49] P. Honvault and J.-M. Launay, J. Chem. Phys. **114**, 1057 (2001).

[50] F. J. Aoiz, L. Bañares, J. F. Castillo, M. Brouard, W. Denzer, C. Vallance, P. Honvault, J.-M. Launay, A. J. Dobbyn, and P. J. Knowles, Phys. Rev. Lett. **86**, 1729 (2001).

[51] D.E. Manolopoulos, J. Chem. Phys. **85**, 6425 (1986).

[52] A.M. Arthurs and A. Dalgarno, Proc. R. Soc. **A 256**, 540 (1960).

[53] E. P. Wigner, Phys. Rev. **73**, 1002 (1948).

[54] R. D. Levine and R. Bernstein, Molecular Reaction Dynamics and Chemical Reactivity, Oxford University Press 1987, p58-59.